Engineering Qualification Model of the SAX X-ray Mirror Unit. Technical data and X-ray imaging characteristics

G.Conti, E.Mattaini, E.Santambrogio
CNR - Istituto Fisica Cosmica - Via Bassini 15 - 20133 Milano - Italy
B.Sacco, G.Cusumano
CNR - Istituto Fisica Cosmica - Via Stabile 172 - 90139 Palermo - Italy
O.Citterio
Osservatorio Astronomico Brera Merate - Via Bianchi 46 - 22055 Merate - Italy
H.Brauninger, W.Burkert
Max Planck Institut fuer Extraterrestrische Physik - D8046 Garching - Germany

ABSTRACT

The scientific instrumentation onboard the Italian X-ray astronomy satellite SAX foresees X-ray imaging Mirror Units (MU) operating in the energy range 0.1 -10 KeV with spatial resolution of 1 arcmin HPR. The MU are composed of thirty nested confocal and coaxial very thin double cone mirrors, made by a nickel electroforming replica technique. The paper presents the results obtained with the Engineering Qualification Model of the MU, which are well within the scientific requirements.

1. INTRODUCTION

The Italian X-ray Astronomy Satellite SAX [1-3], to be launched in mid 1995, is a collaborative program between ASI (Italian Space Agency) and NIVR (Netherlands Agency for Aerospace Programs), and includes six scientific instruments, namely

- a Medium Energy Concentrator/Spectrometer (MECS)
- a Low Energy Concentrator/Spectrometer (LECS)
- an High Pressure Gas Scintillation Proportional Counter (HPGSPC)
- a Phoswich Detector System (PDS)
- two Wide Field Cameras (WFC's).

The scientific requirements of the MECS are: an energy range of 1-10 KeV, effective areas of 240 cm^2 and 150 cm^2 at 1 KeV and 7 KeV respectively, a field of view of 30 arcmin with on axis angular resolution of 1 arcmin Half Power Radius at the centre. To fulfil the effective area requirements, with the allowed dimensions of the satellite, the MECS consists of three identical Medium Energy X-ray Telescopes, each composed of a Mirror Unit (MU) and of a Medium Energy Position Sensitive Gas Scintillation Proportional Counter in the focal plane.

The LECS operates in the extended energy range 0.1-10 KeV, with the same field of view and angular resolution as the MECS, and with an effective area of 80 cm^2 at 1 KeV and 50 cm^2 at 7 KeV and consists of a Mirror Unit and of a Position Sensitive Gas Scintillation Proportional Counter with an ultra thin window at the focal plane.

Thus four identical Mirror Units are foreseen onboard of the SAX satellite, each capable of satisfying both MECS and LECS requirements.

The design of the MU was published in a previous paper [4]. Briefly, it is composed of thirty nested coaxial and confocal mirrors having thickness from 0.2 to 0.4 mm. The mirrors have a double cone geometry to approximate the Wolter I configuration, with diameters ranging from 162 to 68 mm, focal length of 1850 mm and total length of 300 mm. Each MU has a weight of about 13 Kg.

A Development Model of the MU was built at CNR-IFC, Milano and tested for X-ray imaging characteristics at the PANTER X-ray facility with very good results [7].

The Engineering Qualification Model (EQM) is the first complete MU produced by MACDIT, Lecco, in the context of the SAX program, as sub-contractor of LABEN and ALENIA SPAZIO, which is prime contractor for the space segment, and will be followed by the four Flight Models. The present paper summarises the technical data on the EQM and the results of the X-ray tests performed on it at the PANTER facility.

0-8194-1260-0/94/$6.00

2. MIRRORS MANUFACTURING TECHNOLOGY

Due to the large number of mirrors needed for the qualification and for the flight models of the MU and considering the requirements for angular resolution and thickness of the mirror walls, a replica technique by nickel electroforming from mandrels was considered the most appropriate for making the optics. The most critical parameter of the mandrels is the surface roughness, that must be less than 10 Å rms. Two options for mandrels surface finishing were considered during the program development: (a) an acrylic lacquer coating over the aluminium mandrel polished to a roughness of about 50 Å and (b) a superpolished finish to less than 10 Å of an electroless nickel layer deposited on the aluminium mandrel. An extensive series of tests was done [5,6] and the chosen solution was the second one, for reasons of better industrial feasibility and process reliability.

The details of the electroforming technique used for the mirror replica were described in previous papers [5,6] and can be summarised as follows: a 1000 Å thick gold layer is evaporated on the superpolished mandrel to provide the X-ray reflecting surface and to separate the electroless nickel of the mandrel from the nickel of the mirror, deposited in an electroforming bath. The separation of the replicated mirror from the master is accomplished by cooling the aluminium mandrel.

3. MANDRELS

Table 1 lists the nominal values coming from the optical project of the MU. The mechanical tolerances for the mandrels fabrication were defined taking into account the expected MU performances and were the following:

Total mandrel length	$L = L1+L2 = 300 \pm 0.04$ mm
First and second cone length	$L1 = L2 \pm 1$ mm
Maximum diameter	nominal value $\pm$ 0.035 mm
First and second cone angle	nominal value $\pm$ 3 arcsec
Out of roundness	< 0.0015 mm
Slope error	< 6 arcsec rms
Surface microroughness	< 10 Å rms
Maximum damaged surface	1%

The diameters and the angles of the 30 superpolished mandrels used by MACDIT for the production of the mirrors were measured to be within the requested tolerances.

The method used to test the roundness, the profile and the surface roughness of the mandrels during and at the end of the figuring and of the polishing processes, have been already described [8]. The final measured errors and microroughnesses were in accordance with the required specifications. A measure of the surface roughness of the mandrels was also performed with the WYCO-TOPO 2D interference microscope available, from the middle of 1992, at the Brera-Merate Astronomical Observatory. Each mandrel was sampled on 24 points uniformly distributed on the surface, with a magnification factor of 2.5x and the derived microroughness was calculated from a length of 0.66 mm. The survey of the mandrels has given a mean microroughness of 9.9 ± 1.2 Å. It should be noted that these measures were done at the end of the fabrication of the mirrors: from each mandrel at least five mirrors were already been electroformed.

4. MIRRORS

Quality control of the mirror replication process has been implemented by MACDIT by monitoring the physical and chemical parameters inside the gold evaporation chamber and in the nickel electroforming baths. A first check of the geometrical characteristics of a replicated mirror was done on an optical bench at 632 nm wavelength: the mirror was fully illuminated by a parallel or by a slightly divergent beam and the presence of low frequency slope errors due to the manufacturing process was pointed out looking to the shape of the out of focus images produced by the first cone single reflection (divergent beam), by the second cone single reflection and by the double reflection (parallel beam).

To have an assessment of the whole MACDIT production process, 8 mirrors, replicated from 4 different mandrels, were singularly tested at the PANTER facility of MPE on December 91 and March 92. The micoroughness of the 8 mirrors was found to be between 6 and 8 Å rms and the measured Half Power Radius (HPR), i.e. the radius of the circle in which a half of the total image energy is contained, were slightly lower compared to the values calculated by ray-tracing simulations. The same behaviour was noted, in the past, for other mirrors tested during the development phase of the optics [5] and again a similar result comes from the tests presented in this paper, related to a complete MU. The discussion of these results is given in the conclusions.

Number of nested coaxial double-cone mirrors	30
Mirrors overall length	300 mm
First (input) cone length	150 mm
Second (output) cone length	150 mm
Mirror Unit focal length	1850 mm

Mirror number	Maximum diameter (mm)	Medium diameter (mm)	Minimum diameter (mm)	First angle (degrees)	Second angle (degrees)	Thickness (mm)	Collecting area (cm^2)	Weight (Kg)
1	161.873	158.627	148.884	.6200	1.8600	.4	8.172	.527
2	157.680	154.517	145.027	.6040	1.8119	.4	7.754	.513
3	153.636	150.555	141.308	.5885	1.7655	.4	7.362	.500
4	149.743	146.740	137.727	.5736	1.7208	.4	6.994	.488
5	145.850	142.925	134.146	.5587	1.6761	.4	6.635	.475
6	142.107	139.257	130.704	.5444	1.6331	.4	6.299	.463
7	138.365	135.589	127.261	.5300	1.5901	.4	5.972	.450
8	134.772	132.069	123.957	.5163	1.5489	.4	5.666	.439
9	131.179	128.548	120.652	.5025	1.5076	.4	5.368	.427
10	127.737	125.175	117.486	.4894	1.4681	.4	5.090	.416
11	124.444	121.948	114.457	.4768	1.4303	.3	4.831	.304
12	121.301	118.868	111.567	.4647	1.3942	.3	4.590	.296
13	118.159	115.788	108.676	.4527	1.3581	.3	4.355	.288
14	115.016	112.709	105.786	.4407	1.3220	.3	4.127	.281
15	111.874	109.630	102.896	.4286	1.2859	.3	3.904	.273
16	108.732	106.550	100.005	.4166	1.2498	.3	3.688	.265
17	105.590	103.471	97.116	.4046	1.2137	.3	3.478	.258
18	102.448	100.393	94.226	.3925	1.1776	.3	3.274	.250
19	99.306	97.314	91.336	.3805	1.1415	.3	3.077	.242
20	96.165	94.235	88.447	.3685	1.1054	.3	2.885	.235
21	93.322	91.450	85.832	.3576	1.0728	.2	2.717	.152
22	90.480	88.665	83.218	.3467	1.0401	.2	2.554	.147
23	87.638	85.880	80.604	.3358	1.0074	.2	2.396	.143
24	84.796	83.095	77.990	.3249	.9748	.2	2.243	.138
25	81.954	80.310	75.376	.3140	.9421	.2	2.096	.133
26	79.112	77.525	72.763	.3032	.9095	.2	1.953	.129
27	76.271	74.740	70.149	.2923	.8768	.2	1.815	.124
28	73.429	71.956	67.536	.2814	.8442	.2	1.682	.120
29	70.588	69.171	64.922	.2705	.8115	.2	1.555	.115
30	67.746	66.387	62.309	.2596	.7788	.2	1.432	.110

Total geometrical collecting area	123.964 cm^2
Total weight of mirrors	8.702 Kg

Table 1 - Mirror Unit project for SAX MECS and LECS.

5. SPIDERS AND ASSEMBLING

Fig 1 shows the assembled SAX EQM Mirror Unit. Two front end stainless steel spiders with eight arms are supported by a tube on which the flange for the interface to the satellite is mounted. The support and the alignment of the nested mirrors are provided by precise grooves machined on the spiders' arms. For spider production a small milling machine at CNR-IFC Milano was assembled, consisting of a high speed electromandrel (up to 60000 revolutions per minute) that can drive cutters as small as 0.5 mm diameter, and of three micrometric stages (2 translation and 1 rotation), under computer control. The diameters of the obtained grooves were within 5 μm of the nominal requested values; the out of roundness error of a single groove and the mutual concentricity errors of the grooves were better than 5 μm.

Fig 2 shows a detail of an upper spider arm. Before the machining of the mirror grooves, each arm was radially drilled by electroerosion. After the assembling of the whole MU, a pre-set quantity of GE RTV566 silicon compound was syringed along this hole to fix the mirrors and to damp the mechanical vibrations between mirrors and spiders during qualification tests and launch phase.

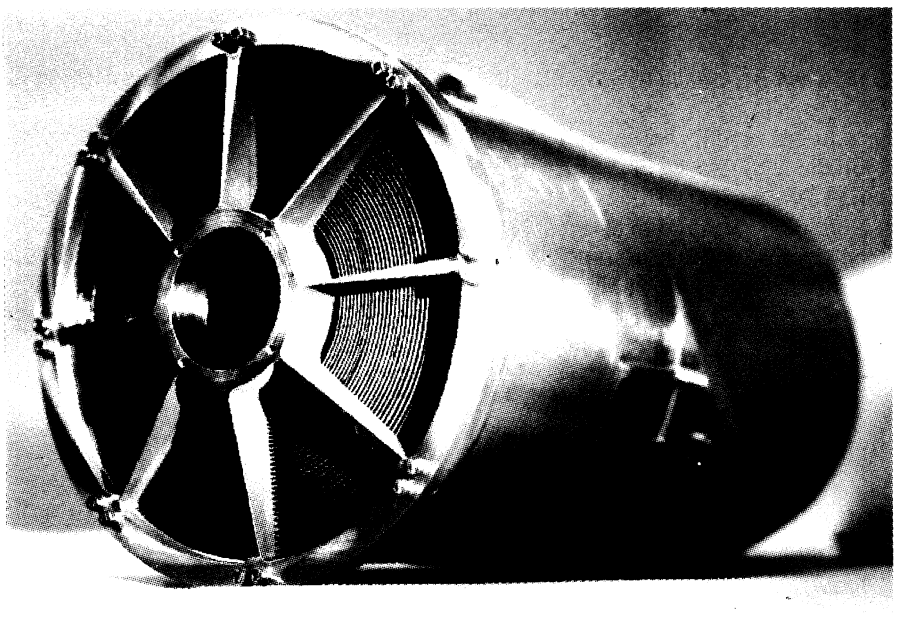

Fig 1 - SAX EQM Mirror Unit

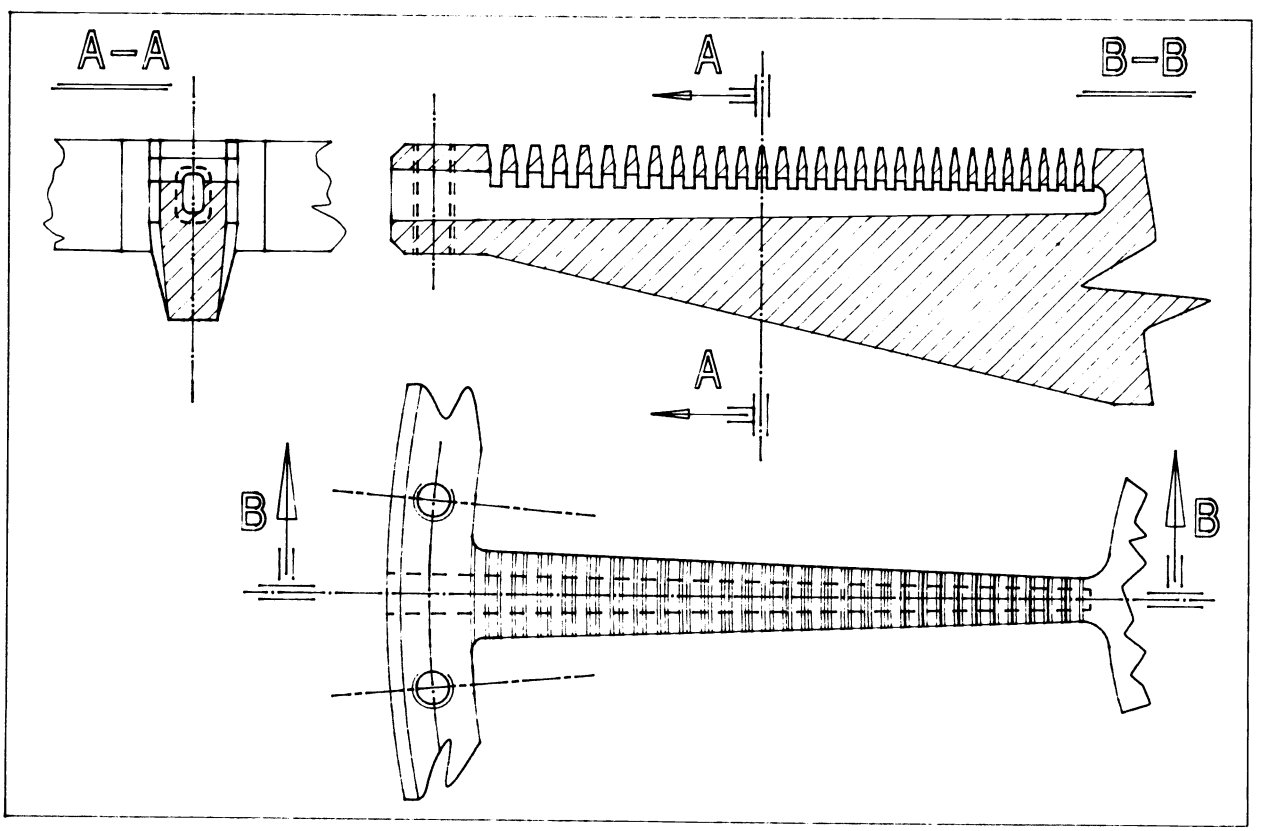

Fig 2 - Detail of an upper spider' arm

6. X-RAY TESTS

6.1 Experimental set-up

The EQM Mirror Unit was tested at the PANTER X-ray facility of Max Plank Institut fuer Extraterrestische Physik, Munich [9,10].

Inside the test chamber, the MU can be horizontally and vertically tilted in order to align its optical axis with respect to the axis of the X-ray beam. On the focal plane optical bench, four detectors from MPE are mounted: the engineering model of the ROSAT Position Sensitive Proportional Counter (PSPC) [11], and three identical polypropylene window proportional counters: the first with a circular 25 mm diameter entrance shield (Open Counter), the other two with 100 μm and 50 μm wide vertical slit entrance shields (Slit Counters). A remote controlled three axis manipulator allows the centring and the focusing of each detector with respect to the image produced by the MU. Moreover, the whole assembly MU-detectors can be horizontally and vertically tilted for off axis measurements. An independent proportional counter, placed at the entrance of the test chamber, is used to monitor the X-ray beam intensity (Monitor Counter).

The measurements were made at 0.3 KeV (C-Kα), 0.9 KeV (Cu-Lα), 1.5 KeV (Al-Lα), 3 KeV (Ag-Lα), 4.5 KeV (Ti-Kα), 6.4 KeV (Fe-Kα), and 8 KeV (Cu-Kα).

6.2 Mirror Unit alignment

The X-rays coming from the PANTER pointlike source 130 m away from the MU, form a divergent beam with a semiaperture of 2.14 arcmin at the input of the outermost mirror and of 0.89 arcmin at the innermost one. The optical design is performed for a parallel input beam and therefore photons coming from a finite distance source and impinging on a small zone near the maximum diameter of each mirror gives rise to a direct reflection (no reflection from the second cone) that forms, at the nominal focal plane, a series of rings around the focalized spot. The innermost of these rings has a diameter of about 32 mm and all are inside the sensitive area of the PSPC detector (80 mm diameter); looking at the symmetry of these direct reflection images, it is possible to align the MU with an estimated accuracy of about 10 arcsec.

The same PSPC was used to position the detectors at the best focus of the MU. The focal distance has been measured at the end of the tests and the obtained value was 1876 ± 1 mm, in accordance with the nominal focal length of 1876.7 mm (value corrected for the finite distance of the source).

6.3 Effective Area measurements

The geometric collecting area of the EQM MU is 123.9 cm^2. The divergence of the beam causes a loss of area because of the above mentioned lack of secondary reflection and because of the mutual shadowing between contiguous mirrors, that amounts to 15.7 cm^2. Spider obstruction also diminishes the useful area by the 10.1% and so the utilised geometrical area for the PANTER tests is 97.3 cm^2.

To measure the effective area, the MU is fully illuminated by the X-ray beam and the Open Counter collects the reflected photons during a fixed interval of time. For the same amount of time the Open Counter is then exposed directly to the incoming beam and the effective area is obtained by the ratio between the reflected and the direct counts, multiplied by the geometrical acceptance area of the detector, with the appropriate normalisation to the Monitor Counter and with the correction due to the different distances from the source to the concentrator and to the detector.

Energy	on axis (cm^2)		5' off axis (cm^2)		10' off axis (cm^2)		15' off axis (cm^2)	
(KeV)	measured	theoretical	measured	theoretical	measured	theoretical	measured	theoretical
0.3	85.9	84.72	75.3	72.21	56.6	54.16	40.0	37.36
0.9	83.1	82.24	71.2	69.95	54.8	52.53	37.6	35.82
1.5	82.1	82.02	73.6	69.86	55.6	52.42	36.5	35.75
3	56.4	47.37	50.8	40.42	36.8	30.00	24.8	21.01
4.5	58.2	58.14	52.4	49.62	38.2	36.88	26.0	25.50
6.4	57.4	53.74	51.3	44.83	35.6	31.01	22.1	20.57
8	37.8	35.83	33.6	28.33	21.5	18.25	13.9	11.63

Table 2 - On axis and off axis Effective Area of SAX EQM Mirror Unit

At each energy the effective area was measured with the assembly MU-detector on axis and at 5', 10', 15' off axis positions. Table 2 lists the obtained values compared with the theoretical ones calculated by ray-tracing simulations, Fig 3 shows the on axis effective area versus energy and Fig 4 shows, as an example, the effective area versus off axis angle at 0.3 and 4.5 KeV, together with the calculated curves. The experimental data have not been corrected to bring the source to infinity and the simulations reproduce the configuration utilized at the PANTER facility. The gold reflectivity curves versus grazing incidence angle and versus energy, used for the simulations, were derived from Zombek [12].

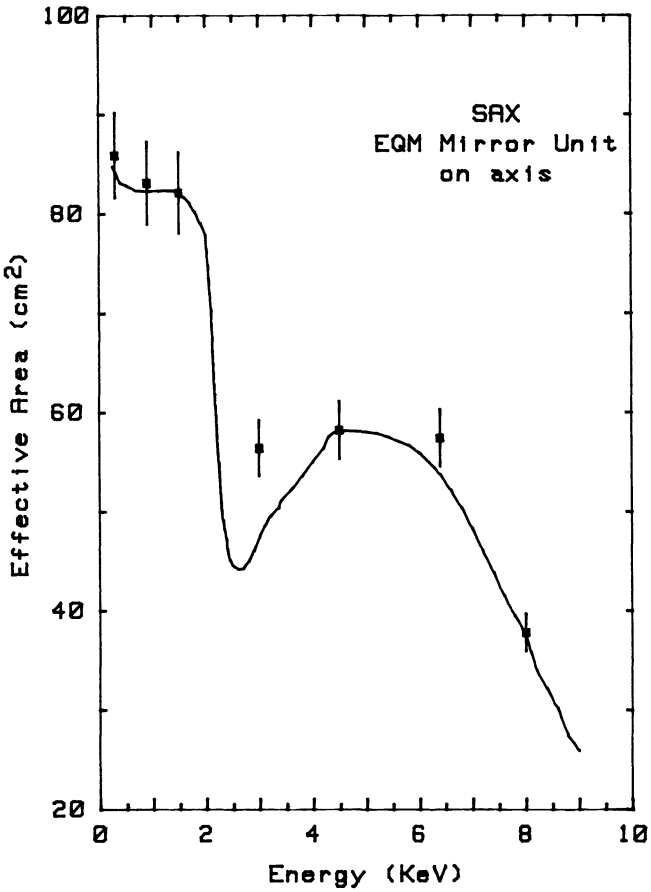

Fig 3. SAX EQM Mirror Unit. Measured and theoretical (solid line) Effective Area vs. X-ray energy.

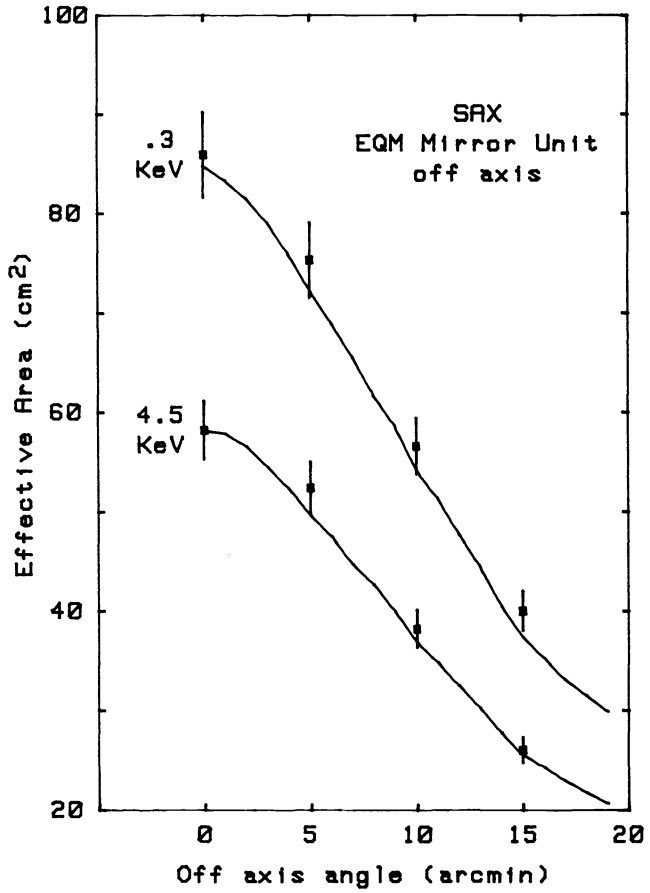

Fig 4. SAX EQM Mirror Unit. Measured and theoretical (solid lines) Effective Areas vs. off axis angle at 0.3 and 4.5 KeV.

A second measure was performed on the EQM MU at the PANTER facility after the vibration tests. A reduced configuration of the facility was available, due to the works in progress to upgrade the PANTER for the XMM requirements and consequently only Effective Area measures were possible. The results have not shown significant variations compared to the data presented in this paper.

6.4 Encircled Energy

The imaging characteristics of the EQM MU were measured with the ROSAT PSPC and with the Slit Counters. The PSPC was used, at each energy, to collect on axis images. Moreover, at 1.5 Kev, off axis images at 5', 10', 15', 20', 25' and 30' were obtained. Fig 5 and 6 show the on axis images at 1.5 KeV and 8 KeV. Fig 7 shows two images at 1.5 KeV, obtained with 1 arcmin tilt of the MU-detector assembly after one half of the integrating time. The dimensions of the images are 250 x 250 pixels and the plate scale factor is 22 μm/pixel (2.4 arcsec/pixel).

With the 100 μm Slit Counter, a scan across the on axis image at the focal plane was performed between -12 mm and 12 mm from the peak, at each energy. The scan step was 50 μm for the 4 mm around the peak and 100 μm for the outer parts; in each position the detector accumulates counts for a fixed time interval.

The imaging characteristics of a MU are defined by the Encircled Energy Function (EEF) that is the fraction of total energy at the focal plane contained in a circle of radius r, versus r. The EEF is derived from the Point Spread Function (PSF), the intensity function of a point source imaged by the MU. The slit scan (SLF) is the PSF integrated in one direction. The EEF can be derived directly by integration on a PSPC image but the spatial resolution of the PSPC is energy-dependent. With the hypothesis of a circular symmetry of the image, well verified in our case, the PSF and then the EEF can be derived from the SLF. Each of them is fitted with the sum of the following functions in which G_i and B_i are free parameters of the fit:

$$SLF(x) = \sum_{i=1,4} 0.5G_i/(B_i(1+(x/B_i)^2)^{3/2}))$$

The corresponding PSF is: $$PSF(r) = \sum_{i=1,4} G_i/(\pi B_i^2(1+(r/B_i)^2)^2)$$

which verify the relation: $$SLF(x) = \int_{-\infty}^{+\infty} PSF(r)dy \qquad \text{with} \qquad r^2=x^2+y^2$$

The EEF is then: $$EEF(r) = \int_0^{2\pi}\int_0^{r} PSF(r)rd\theta dr = \sum_{i=1,4} G_i(1-1/(1+(r/B_i)^2))$$

The choice of these particular functions to fit the slit scans data, has been verified using the 1.5 KeV image of the PSPC because at this energy the spatial resolution of the PSPC is comparable with the 100 μm Slit Counter. On the image a slit scan has been simulated and the obtained data have been fitted with the above described functions. The resulting EEF was in very good agreement with the EEF directly integrated on the image (the difference of the two estimated 50% energy radius is less than 1%).

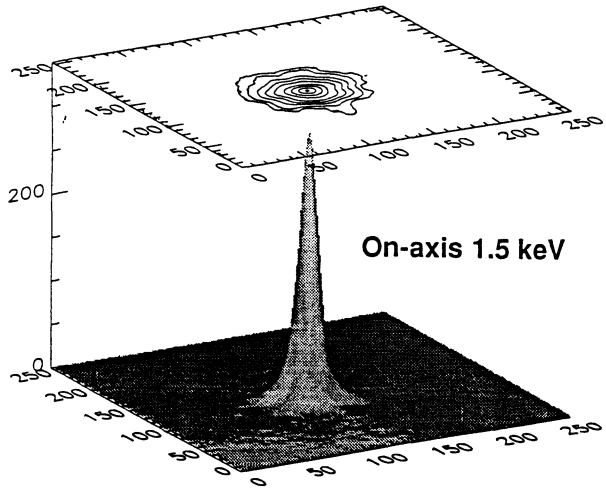

Fig 5 - SAX EQM Mirror Unit. On axis image of a 1.5 KeV pointlike source (ROSAT PSPC). X Y units are pixels.

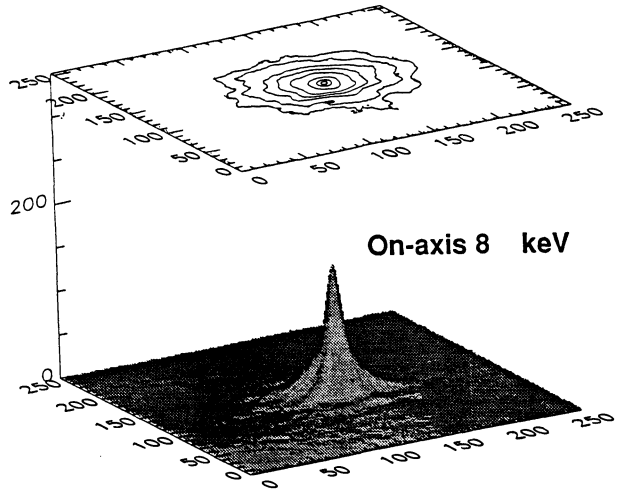

Fig 6 - SAX EQM Mirror Unit. On axis image of a 8 KeV poitlike source (ROSAT PSPC). X Y units are pixels.

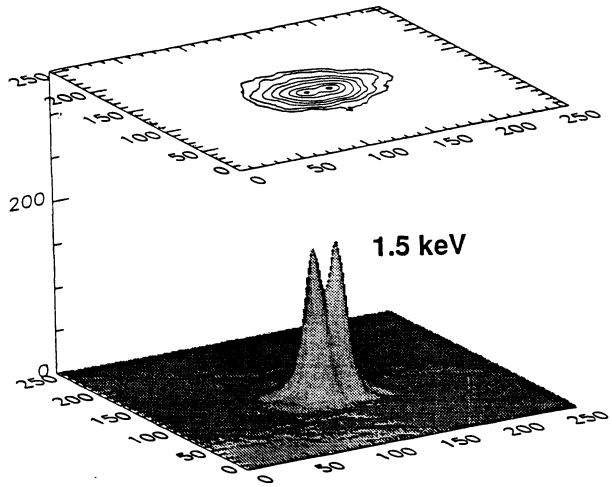

Fig 7 - SAX EQM Mirror Unit. Image of two 1.5 KeV pointlike sources separated by 1 arcmin (ROSAT PSPC). X Y units are pixels with a scale factor of 2.4 arcsec/pixel.

Table 3 lists the values of the 50%, 80% and 90% energy radius calculated, as above described, from the measured slit scans (columns (a)). The data are compared with two sets of theoretical values obtained by ray-tracing simulations. The first (columns (b)) is calculated considering a perfect double cone geometry and the scattering produced by the surface roughness.

The second one (columns (c)), takes into account the scattering and a "daisy" deformation of the mirrors: the last 50 mm of the mirrors, beginning from the maximum and minimum diameters, have been deformed progressively in such a way to have at the two ends a sinusoidal variation of the circular cross section with amplitude of 5 μm peak to peak and periodicity that corresponds to the distance of two successive arms of the spiders. This is the most likely deformation to appare after the integration of the mirror shells into the MU.

As for Effective Area, the measured data have not been corrected to bring the source to infinity and the theoretical values have been calculated for a source 130 m away from the MU; the used focal length is therefore 1876 mm. The aim of these tests was not to give a calibration of the MU, that will be done, together with the MECS and LECS detectors, for the flight units. The ray-tracing simulations have been repeated, at 1.5 KeV, with an infinite distant source and the difference between the obtained 50%, 80% and 90% energy radius and the values in Table 3 is of the order of +1 arcsec.

Energy (KeV)	R50% (arcsec)			R80% (arcsec)			R90% (arcsec)		
	measured (a)	theoretical (b)	theoretical (c)	measured (a)	theoretical (b)	theoretical (c)	measured (a)	theoretical (b)	theoretical (c)
0.3	27.4	32.4	28.7	60.0	54.8	60.6	91.6	67.0	100.7
0.9	28.5	32.8	28.5	63.0	55.7	61.0	96.3	68.1	99.8
1.5	29.3	33.3	29.2	64.9	56.1	62.6	99.3	69.1	106.8
3	31.8	34.1	31.0	73.0	60.0	71.3	112.3	85.6	123.5
4.5	35.1	36.5	35.5	89.2	68.4	92.6	155.4	112.6	138.1
6.4	38.1	39.6	38.2	107.0	85.1	108.5	180.6	138.6	155.5
8	38.8	38.2	38.4	111.6	98.0	118.4	188.4	150.1	169.4

Table 3 - Measured and theoretical 50%, 80% and 90% energy radius: - (a) measured values on SAX EQM Mirror Unit - (b) theoretical values with nominal double cone geometry + scattering - (c) theoretical values with deformed geometry (daisy effect) + scattering.

Off axis angle (arcmin)	R50% (arcsec)
0	29.3
5	27.1
10	28.3
15	39.2
20	62.1
25	93.4
30	119.6

Table 4 - SAX EQM Mirror Unit. Off axis measured 50% energy radius at 1.5 KeV (ROSAT PSPC).

Table 4 lists the 50% energy radius derived from the ROSAT PSPC off axis images at 1.5 KeV; the EEF is calculated by integration on a 24 mm diameter circle centred on the peak.

Fig 8 shows the EEF measured at 0.3 KeV together with the theoretical EEF derived from a simulation with nominal double cone geometry and no scattering. Fig 9 and Fig 10 show the EEF derived from slit scans respectively at 0.9; 3; 8 KeV and 1.5; 4.5; 6.4 KeV.

7. DISCUSSION AND CONCLUSIONS

The measured on axis and off axis effective areas are in good agreement with the theory, with the exception of the value at 3 KeV that is higher than expected. The explanation is that this energy is near to the absorption edge of the gold and the simulations are done with monochromatic energy values, while the Ag-Lα line is contaminated by lower energies continuum. It would be interesting to have, for the calibrations of the MECS and LECS flight units, more experimental data in the range 1.5 - 4.5 KeV to have better information about the Effective Area in this critical zone of the energy spectrum.

The obtained values for the 50% energy radius (HPR) are well within the required specifications over whole energy range.

With reference to the experimental and theoretical data in Table 3, it should be noted that the double cone approximation of Wolter I mirror configuration suffers from intrinsic spherical aberration, which means that the intersection length of a reflected ray with the optical axis depends on the distance of the input ray from the optical axis. Therefore, from the point of view of geometrical optics, a point source is imaged, by each mirror in a circle of least confusion. Deformations from ideal double cone configuration are present mainly at the front and back ends of the mirrors, caused by the residual stresses in the electroformed optics and by the mechanical coupling between the mirrors and the spiders (daisy effect). These zones of the mirrors contributes to the outer part of the image blur circle and therefore a deformation will spread part of the reflected X-rays toward the centre of the image and part outside of the geometrical circle of least confusion, with the effect to produce a better

50% and a worst 80% and 90% energy radius with respect to the nominal ones.

This hypothesis is confirmed by the comparison of experimental and theoretical data of the 50% energy radius in Table 3: there is a good agreement between the measured values (column (a)) and the results of the simulations that take into account the scattering and the geometrical deformations of the mirrors (column (c)), while the experimental data are lower than the theoretical ones listed in column (b) that considers only the scattering due to surface roughness. The agreement is also good between the data in columns (a) and (c) of the 80% energy radius while the measured values in column (a) are higher than the expected ones listed in column (b). Again for the 90% energy radius the same correspondence found for he 80% is confirmed although the agreement between data in columns (a) and (c) is not good as a consequence of the fact that the results of this simulation depend strongly from the type of geometrical deformation considered.

From slit scan data at 8 KeV and 0.3 KeV it is possible to evaluate the ratio between the scattered and the reflected X-rays and then to derive a mean surface roughness [13]. The obtained value for the EQM MU is 8.4 Å rms.

8. ACKNOWLEDGEMENTS

We wish to thank G.Boella and L.Scarsi for supporting and encouraging our work and R.C.Butler, SAX payload manager, for helpful discussions. R. Valtolina, from OAB, has performed the WYCO roughness measurements. The technical staff of MACDIT, LABEN and ALENIA SPAZIO industries have given an active collaboration.

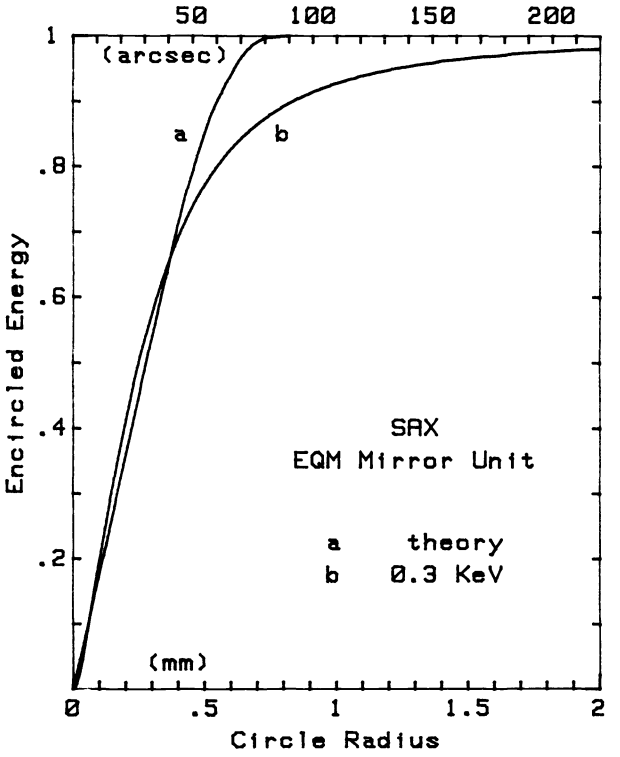

Fig 8 - SAX EQM Mirror Unit. Measured Encircled Energy Function at 0.3 KeV. The theoretical curve is calculated for a nominal double cone geometry and with no scattering.

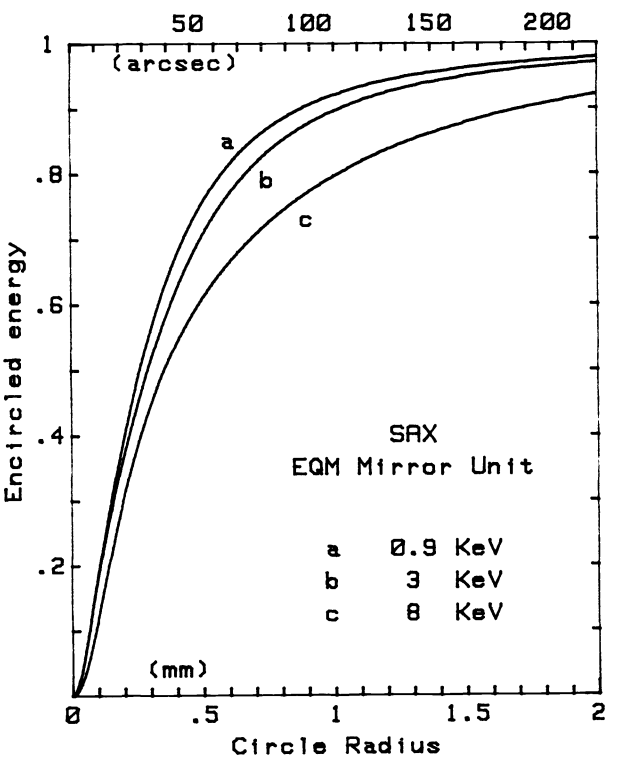

Fig 9 - SAX EQM Mirror Unit. Measured EEF at 0.9, 3 and 8 KeV.

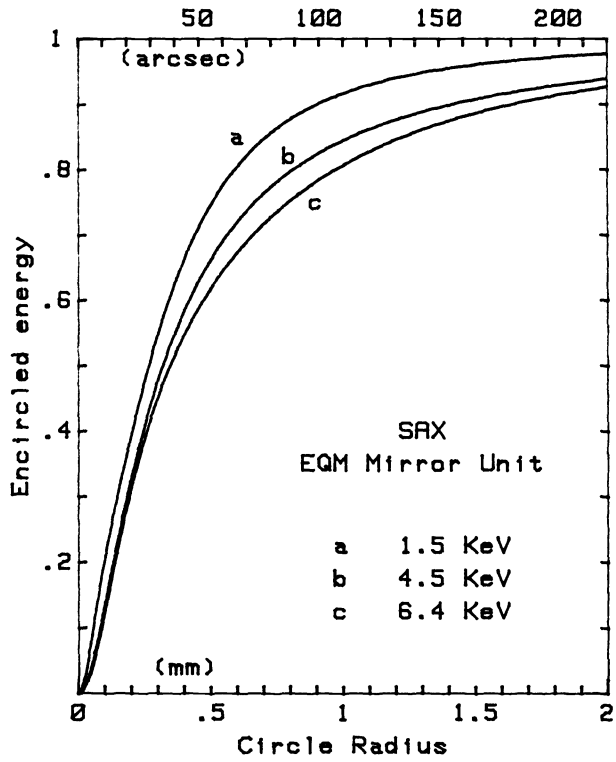

Fig 10 - SAX EQM Mirror Unit. Measured EEF at 1.5, 4.5 and 6.4 KeV.

9. REFERENCES

(1) L.Scarsi, "The SAX mission," Adv. Space Res. 3, 491 (1984).

(2) G.Spada, "SAX Scientific Instrumentation," in Proceedings, Conference on Non thermal and Very High Temperature Phenomena in X-Ray Astronomy, Rome (1983) pp 217-234.

(3) C.Perola, "The Scientific Objectives of the SAX Mission," in Proceedings, Conference on Non thermal and Very High Temperature Phenomena in X-Ray Astronomy, Rome (1983) pp 173-230

(4) O.Citterio, G.Conti, E.Mattaini, B.Sacco and E.Santambrogio, "Optics for X-ray Concentrators on Board the Astronomy Satellite SAX," Proc. SPIE 597, 102 (1985).

(5) O.Citterio, G.Bonelli, G.Conti, E.Mattaini, E.Santambrogio, B.Sacco, E.Lanzara, H.Brauninger and W.Burkert, "Optics for the X-Ray Imaging Concentrators Aboard the X-Ray Astronomy Satellite SAX," Appl. Opt. 27, 1470 (1988)

(6) G.Conti, G.Bonelli, E.Mattaini, E.Santambrogio, O.Citterio, H.Brauninger and W.Burkert, "Lacquer Coated Mandrels for Production of Replicated X-Ray Optics," Proc. SPIE 1140, 376 (1989).

(7) O.Citterio, P.Conconi, G.Conti, E.Mattaini, E.Santambrogio, G.Cusumano, B.Sacco, H.Brauninger and W.Burkert, "Imaging Characteristics of the Development Model of the SAX X-Ray Imaging Concentrator," Proc. SPIE 1343, 145 (1990).

(8) G.Bonelli, G.Conti, E.Mattaini and O.Citterio, "Characterisation of the Mandrels used to produce Replicated Prototypes Mirrors for the Italian X-Ray Satellite SAX," Proc. SPIE 830, 44 (1987).

(9) B.Aschenbach, H.Brauninger, K.H.Stephan and J.Trumper, "X-Ray Test Facilities at Max Planck Institute, Garching," Proc. SPIE 184, 234 (1979).

(10) K.H.Stephan, P.Predhel, B.Aschenbach, H.Brauninger and A.Ondrusch,"Soft X-Ray Source for the Max Planck Institute (MPI) Long Beam (130 m) Test Facility," Proc. SPIE 316, 203 (1981).

(11) U.Briel and E.Pfefferman, "The Position Sensitive Proportional Counter (PSPC) of the ROSAT Telescope," Nucl. Instr. and Meth. A242 (1986), 376.

(12) M.V.Zombek, AXAF Interim Rep. SAO-AXAF016 (1983).

(13) P.Beckmann and A.Spizzichino, The Scattering of Electromagnetic Waves from Rough Surfaces Pergamon, New York, (1963).